GUIDOTTIITE, THE Mn-ANALOGUE OF CRONSTEDTITE: A NEW SERPENTINE-GROUP MINERAL FROM SOUTH AFRICA

MICHAEL W. WAHLE[1], THOMAS J. BUJNOWSKI[1], STEPHEN GUGGENHEIM[1,*], AND TOSHIHIRO KOGURE[2]

[1] Department of Earth and Environmental Sciences, University of Illinois at Chicago, Chicago, Illinois 60607 USA
[2] Department of Earth and Planetary Science, Graduate School of Science, The University of Tokyo, 7-3-1 Hongo, Bunkyo-ku, 113-0033, Tokyo, Japan

Abstract—The objective of this paper is to describe the new serpentine group mineral, guidottiite, which is analogous to cronstedtite. Guidottiite has an ideal chemical composition of $(Mn_2Fe^{3+})(SiFe^{3+})O_5(OH)_4$. The sample is from the N'chwaning 2 mine, Kalahari manganese field, Republic of South Africa, and apparently forms from hydrothermal solutions. Grains are optically near opaque [average index of refraction 1.765, with variable extinction on the (001)], vitreous, and black, with perfect {001} platy cleavage. A non-separable fibrous substructure exists perpendicular to cleavage that results in a silky luster under optical examination. The average chemical analysis determined from electron microprobe based on four grains with ten analyses each resulted in a structural formula of $(Mn_{1.86}Fe^{3+}_{0.61}Mg_{0.54})_{\Sigma=3.01}$ $(Si_{1.36}Fe^{3+}_{0.64})_{\Sigma=2.00}O_5(OH)_4$, with calculated density of 3.236 g/cm^3. Analysis from another area of the sample showed a slightly different chemical composition and resulted in a formula of $(Mn_{1.70}Fe^{3+}_{0.96}Mg_{0.24})_{\Sigma=2.89}(Si_{1.26}Fe^{3+}_{0.74})_{\Sigma=2.00}O_5(OH)_4$, with calculated density of 3.291 g/cm^3. The measured density on a bulk sample (with impurities) was 3.33 g/cm^3. Thermal analysis suggested a dehydroxylation temperature of 535ºC, a decomposition/recrystallization temperature of 722ºC, and weight loss (= H_2O loss) of 9.4%. The derived Mohs hardness from nano-indentation is H = 4.25.

The sample is mostly the $2H_1$ polytype with minor amounts of the $2H_2$ polytype. Using a predominantly $2H_2$ crystal, which has better crystallinity, the strongest observed X-ray peaks are: 7.21 Å (I_o/I_o = 100%), 3.543 (50), 2.568 (39), 1.982 (26), and 2.381 (25). All Gandolfi simulations, even with three crystal remountings, showed preferred orientation effects. Transmission electron microscope (TEM) analysis showed stacking disorder within Group D serpentine polytypes. Thus, a regular alternation of the occupancy of octahedral sets within each layer along the stacking exists, but disorder of the layer displacements of 0 and $\pm b/3$ (*b* defined here as the orthohexagonal cell) exists. Ordered $2H_1$ (no layer displacement) and $2H_2$ (alternating + and $-b/3$ displacement) domains were also frequently observed. X-ray diffraction analysis showed that even apparent single crystals contain impurity phases, presumably Mn-rich and Ca phases that were detected in the microprobe study. The single-crystal structure refinement used a well (stacking) ordered apparent $2H_2$ crystal with little to no streaking in the diffraction pattern. Results showed that the crystal has a random interstratification of $2H_2$ and $2H_1$. The $2H_2$ polytype is hexagonal, space group $P6_3$, with a = 5.5472(3), c = 14.293(2) Å, and Z = 2, and was refined to R_1 = 0.072 and wR = 0.108 from 656 unique reflections. Because the two polytypes in the composite have only small differences in the lower 1:1 layer, a large displacement parameter for the basal oxygen atom results, which was constrained to B = 1.5 Å^2 (U_{eq} = 0.0190) in the refinement. Half of the tetrahedral sites in the $2H_1$ upper layer superpose over half of the tetrahedral sites in the $2H_2$ upper layer (T1 sites only) per unit cell. This superposition produces an apparent excess of electron densities of the T1 site relative to the T2 site (T1 = 21.9 electrons, T2 = 15.8). Comparison with the microprobe data indicates that observed tetrahedral bond lengths are generally not affected by this intergrowth. Tetrahedral bond lengths indicated that the tetrahedral sites contain T1 = $Si_{0.678}Fe^{3+}_{0.322}$ and T2 = $Si_{0.631}Fe^{3+}_{0.369}$. This excess of electron densities and other refinement problems associated with the guidottiite single-crystal refinement closely parallel all single-crystal cronstedtite-$2H_2$ refinements to date, suggesting that these refinements also involve random interstratifications of $2H_2$ and $2H_1$ polytypes.

Key Words—Composition, Cronstedtite, Crystal Structure, Density, Guidottiite, Physical Properties, Serpentine, Thermal Analysis, Transmission Electron Microscopy, X-ray Diffraction.

INTRODUCTION

In 1993, Dr Ludi von Bezing of Kimberly, South Africa, sent a sample of a Mn-rich serpentine to the corresponding author. Examination of the sample showed that the material was a new mineral that is analogous to cronstedtite, an Fe-rich trioctahedral 1:1 layer silicate of the serpentine group with an ideal end-member formula of $(Fe^{2+}_2Fe^{3+})(SiFe^{3+})O_5(OH)_4$. For the Mn-rich serpentine, data on the physical, chemical, thermal, and optical properties, occurrence, and polytype structure using transmission electron microscopy and X-ray diffraction are provided. In recognition of the late

Charles V. Guidotti (1935−2005) of the University of Maine, USA, for his many contributions to phyllosilicate mineralogy, this Mn-rich end-member mineral is named guidottiite (gwi dot′ ē īt). A sample (NMNH 174879) has been deposited in the Smithsonian Institution, Washington, D.C., and the new species and name have been approved by the International Mineralogical Association (# 2009-061).

The twelve standard polytypes (not including enantiomorphic pairs) of the serpentine group minerals (Zvyagin, 1962; Bailey, 1969; Dornberger-Schiff and Ďurovič, 1975) are formed by various layer displacements in the stacking of the 1:1 layers and by the occupancy of octahedral sets within each layer. Of these polytypes, eight ($1T$, $3T$, $2H_1$, $2H_2$, $2T$, $1M$, $2M_1$, and $3R$) have been described for cronstedtite and three were studied by single-crystal X-ray methods: (1) a cronstedtite-$3T$ crystal (Smrčok et al., 1994), (2) two cronstedtite-$1T$ crystals (Hybler et al., 2000), and (3) three cronstedtite-$2H_2$ crystals (Geiger et al., 1983; Hybler et al., 2002). Cronstedtite-$2H_2$ structure refinements are problematic in that the observed mean tetrahedral bond lengths suggest a composition that differs significantly from the observed electron density for each site. Several explanations, such as twinning of many types and polytype intergrowths, have been proposed to justify these results, but little supporting evidence exists as to how these possible explanations may affect the apparent chemical composition of the tetrahedra and the structure refinement.

Like cronstedtite, guidottiite-$2H_2$ shows apparent inconsistencies associated with tetrahedral bond lengths and observed electron densities. The sample is composed of two polytypes, the $2H_1$ and $2H_2$ forms, and the $2H_2$ structure was investigated in more detail. Unlike previous studies of cronstedtite-$2H_2$, the possible effects of twinning and polytype intergrowths are considered in detail to account for the inconsistencies. The best model for the apparent guidottiite-$2H_2$ structure is one where an incoherent intergrowth (i.e. a random interstratification) exists of $2H_2$ and $2H_1$. The results closely parallel cronstedtite-$2H_2$ refinements and, thus, a similar intergrowth probably occurs for cronstedtite.

OCCURRENCE

Guidottiite was found in a pocket in the N'chwaning 2 mine, northern section, northern development drive, Kalahari manganese field, Republic of South Africa, at floor contact ~15 y ago. The Kalahari field is located in the northern Cape province. The occurrence is ~45 m from the boundary of the Wessels mine claim area. The ore bodies are three conformably layered manganese bands alternating with jasper-hematite lutite, with only the bottom manganese layer being mined at the time of the find. This layer averages ~3−5 m in thickness in this area of the Kalahari field. A review of the Proterozoic

stratiform manganese deposits, including the Kalahari field, is presented by Schissel and Aro (1992).

Pockets are unusually close in contact or near faults with thin bands of ore apparently relating to injection or percolating hydrothermal solutions. Brecciated areas near the faults are commonly extensively mineralized. The paragenesis of guidottiite is a layered sequence of hematitic ore-chlorite(?)-guidottiite-chlorite(?)-leuco-phoenicite/caryopilite(?)-barite-rhodochrosite-shigaite-gageite.

PHYSICAL PROPERTIES

The sample as received appeared to be pure guidottiite, without any associated minerals, and was columnar in appearance. Guidottiite grains, ranging in size up to ~3 mm, were poorly cemented; gentle crushing separated the grains. The grains are vitreous and black, with perfect (001) cleavage. Light from a strong source and reflecting from grain surfaces under microscope examination at ~3 × shows a very fine (non-separable) fibrous structure, perpendicular to cleavage, resulting in a silky luster. Surfaces lateral to the cleavage show occasional rounded prominences, suggesting an apparent subconchoidal fracture, though this feature appears to be related to original grain shape and not fracture. Besides the perfect (001) cleavage, no additional crystallographic preference for cleavage or fracture exists. The grains were too small to determine Mohs hardness directly. A sample, mounted in epoxy resin and polished, was used for nano-indentation tests. Seventeen locations on grains of various orientations were tested to indentation depths to 400 nm; hardness depended on indentation depth, with limited variations of hardness at shallow depths. The representative hardness, H, is 3.75 (GPa = 388 kg/mm^2). Based on the tables in Broz et al. (2006), this result correlates to a Mohs hardness of 4.25.

OPTICAL PROPERTIES

Crystals are very light-absorbent and only become optically transparent where crystal thickness is <20 μm. The smallest crystal that could be obtained and still conveniently manipulated was ~65 μm × 90 μm × 15 μm in size. Dimensions smaller than 20 μm could only be obtained by utilizing the perfect (001) cleavage. Similarly sized grains for both the $2H_1$ and $2H_2$ polytypes (see X-ray crystallography) were mounted on glass fibers for spindle-stage examination. Each grain was rotated to align the (001) plane (15 μm dimension) with the microscope stage to determine the two refractive indices in (001). Unfortunately, no observable retardation occurs at this thickness, and thus only an approximate index of refraction could be determined, based on the immersion method in white light, at an index of refraction of 1.765. Crystals exhibit some

retardation upon rotation on the spindle stage. In plane-polarized light, the (001) plane exhibited a honey-yellow color and no apparent pleochroism. Both the $2H_1$ and the $2H_2$ polytypes exhibited similar absorption, colors, and refractive index. Crystals of both polytypes showed domains with different extinctions on the (001). The black color of the crystal and its opaque character prevented optical determination of any twinning.

COMPOSITION

Analyses were made by M. Yates, University of Maine-Orono and J. Alt, University of Michigan, both using Cameca electron microprobes, hereafter referred to as Cameca-Y and Cameca-A, respectively. The samples analyzed were inhomogeneous, although samples were chosen based on apparent homogeneity. Domains present included low and high Mn-rich and high Ca phases. Pure areas could be identified and analyzed. Microprobe analyses did not differentiate between polytypes. Both instruments indicated that Al, Ca, Cr, K, Na, P, S, and Ti were below detection limits, and the Cameca-Y instrument also found that Cl was present at 0.15 ± 0.02 wt.%.

The Cameca-Y analyses involved nine locations, with ten analyses at each location. The conditions were 15 kV, 10 nA, and a defocused 5 μm beam; the standards used were diopside for Si and Mg, rhodonite for Mn, magnetite for Fe, and scapolite for Cl, with 10 s counting time for each element on both standards and unknowns. Fe was analyzed as Fe_2O_3, Mn was analyzed as MnO, and H_2O was estimated for use in matrix corrections. The Cameca-Y analyses resulted in (oxide wt.%): MgO, 5.65 ± 0.79; MnO, 34.21 ± 0.84; Fe_2O_3, 25.97 ± 0.22; SiO_2, 21.23 ± 0.44; total = 87.06. The analyses produced the following structural formula, determined anhydrously, based on seven oxygen atoms: $(Mn_{1.86}Fe^{3+}_{0.61}Mg_{0.54})_{\Sigma=3.01}$ $(Si_{1.36}Fe^{3+}_{0.64})_{\Sigma=2.00}O_5(OH)_4$. The valence states of Fe and Mn are somewhat uncertain, and require further analysis; by analogy to cronstedtite, Fe^{3+} and Mn^{2+} were assumed. The Cameca-A instrument involved three spots on one grain and resulted in the following: MgO, 2.49; MnO, 30.90; Fe_2O_3, 34.85; SiO_2, 19.36, Total = 87.60, with a formula of $(Mn_{1.70}Fe^{3+}_{0.96}Mg_{0.24})_{\Sigma=2.89}(Si_{1.26}Fe^{3+}_{0.74})_{\Sigma=2.00}$ $O_5(OH)_4$. The analytical conditions were 15 kV, 10 nA, defocused 10 μm beam, rhodonite standard for Mn, and a glass standard for the remaining elements.

DENSITY

The density was determined using a 2 mL pycnometer using diiodomethane (ρ = 3.325 g/cm^3) liquid and a miscible solid, iodoform (ρ = 4.008 g/cm^3), following the suspension method (*e.g.* Bloss, 1971, p. 346). Optical examination of the guidottiite grains in the liquid column was used to determine that the specific gravity of the liquid matched exactly that of the grains; the

grains remained motionless in the liquid. The grains examined varied in size between 0.3 and 1 mm in plan and were chosen based on the apparent lack of splitting and no apparent inclusions. The measured density is 3.33 g/cm^3, with an estimated error in precision of ±0.01. The calculated density is 3.236 g/cm^3 using the composition determined from the Cameca-Y probe results and 3.291 g/cm^3 if calculated from the Cameca-A results. The density results suggest that significant impurity phases are present, as determined also in the chemical analysis.

THERMAL ANALYSIS

Differential thermal analysis (DTA) involved a high-pressure apparatus (Koster van Groos, 1979; Guggenheim and Koster van Groos, 1992) that was operated at 1 bar (room pressure). Approximately 10 mg of sample was placed in a gold capsule that remained open to the atmosphere during the experiment. The experimental conditions included ramp heating using a programmable controller at a rate of 20°C/min as measured by a $Pt-Pt_{90}Rh_{10}$ thermocouple and recorded on a Kipp strip chart at the 50 μm setting. An 18 mg Al_2O_3 + 2 mg quartz reference was used, and the temperature of the sample was obtained by using the temperature of the reference after correcting for the differential temperature. The DTA pattern (Figure 1a) shows an endothermic peak temperature of 535°C (extrapolated onset temperature of 495°C, extrapolated return temperature of 570°C), and an exothermic peak temperature at 722°C (extrapolated onset temperature of 706°C, extrapolated return temperature not determined). The 535°C peak is interpreted as resulting from dehydroxylation and the 722°C peak from decomposition/recrystallization.

Thermal gravimetric analysis (TGA) was performed using a Dupont TGA 951 instrument. Approximately 20.15 mg of sample was analyzed at a heating rate of 10°C/min under ultra-dry N_2 at a flow rate of 500 cc/min. Significant weight loss (Figure 1b) occurred between 384°C and 560°C. This temperature range approximates the range determined by DTA for the low-temperature reaction, which was interpreted as relating to dehydroxylation. Assuming that weight loss at lower temperatures is related to adsorbed (surface) water, the weight loss owing to dehydroxylation was ~6.6%. If total water is considered (*i.e.* total weight loss to 560°C), the loss in weight was 8.4%. The total weight loss based on the temperature at 999°C was 9.1% and based on the (extrapolated) temperature at 1100°C is 9.4%. The calculated H_2O content for the ideal formula of $(Mn_2Fe^{3+})(SiFe^{3+})O_5(OH)_4$ was 9.1%, and the calculated H_2O content for the Cameca-Y-derived composition was 9.4%. Differences from the microprobe sums may relate to uncertainty in the valence states of Fe and Mn.
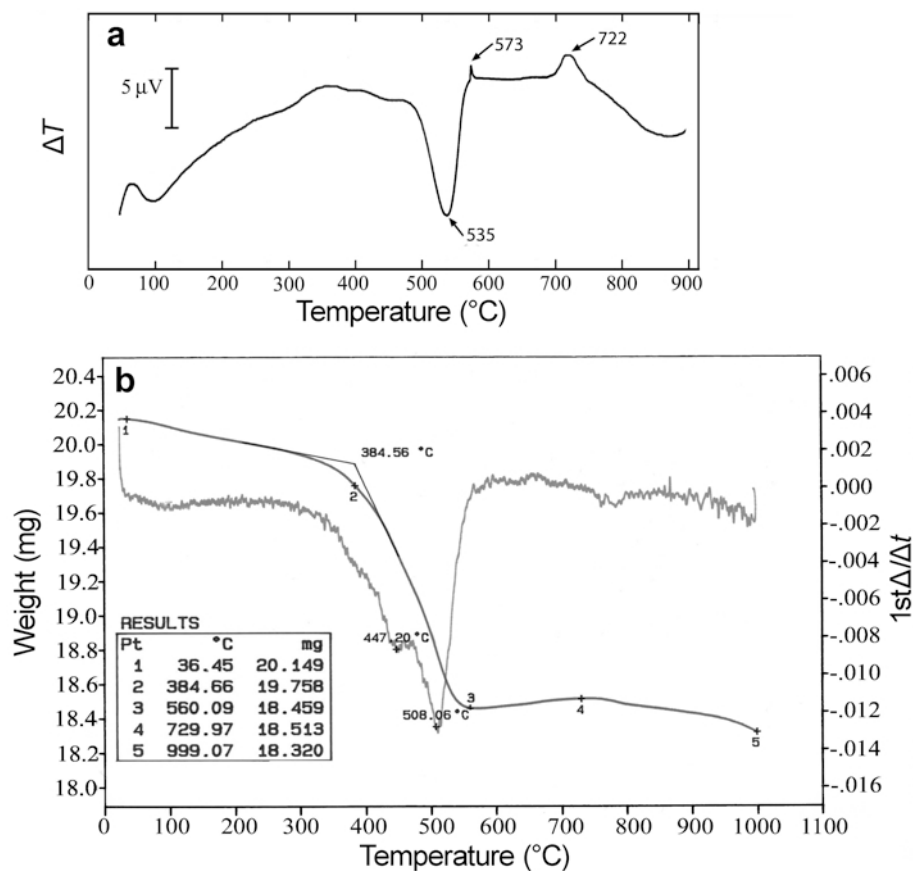
Figure 1. (a) Differential thermal analysis (DTA) of guidottiite. The peaks represents dehydroxylation (535ºC), quartz transformation (573ºC) and decomposition (722ºC). (b) Thermal gravimetric analysis (TGA, weight scale shown on left) and the first derivative of the curve (scale on right) of guidottiite.

TRANSMISSION ELECTRON MICROSCOPE (TEM) ANALYSIS

Each specimen for TEM examination was prepared by gently crushing a grain and then embedding the crushed sample in epoxy resin between two glass slides (Kogure, 2002). After hardening, the glass slides were cut into laths ~1 mm thick using a diamond wheel. The laths were thinned to ~50 μm by mechanical grinding and then argon-ion milled. The TEM analysis was performed at 200 kV using a JEOL JEM-2010 UHR with a nominal point resolution of 2.0 Å. Selected-area electron diffraction (SAED) patterns were recorded using a Gatan ES-500W side-mounted CCD camera. Energy-dispersive X-ray spectroscopy (EDS) was performed using a JEOL JED-2200 system attached to the TEM. High-resolution TEM (HRTEM) images were recorded on film or a Gatan MSC 794 bottom-mounted CCD camera. Contrast is believed to correspond to the projected potential of the crystal structure (Kogure, 2002) because HRTEM images were obtained at sufficiently thin regions of the specimen and images were taken by adjusting the objective lens near Scherzer

defocus. Noisy contrast from amorphous materials in HRTEM images was removed using a Wiener-filter (Marks, 1996; Kilaas, 1998) developed by K. Ishizuka (HREM Research Inc.) and implemented with Gatan *DigitalMicrograph* version 3.10.0 (Kogure *et al.*, 2008).

The SAED patterns, using a selected-area aperture with a diameter corresponding to ~100 nm, and with the incident beam along the <100> directions, show various features (Figure 2a−c). The 01l and 02l reflection rows show two-layer periodicity (Figure 2a), one-layer periodicity (Figure 2b), or a heavily streaked pattern (Figure 2c). In contrast, SAED patterns along the <1$\bar{1}$0> directions always show the same orthogonal lattice with two-layer periodicity and no streaking, regardless of the patterns along the <100> directions (Figure 2d). These results indicate that all stacking sequences in the crystal belong to group D (Bailey, 1969), but locally the stacking is an ordered 2H_2 (Figure 2a) or 2H_1 (Figure 2b), both of which are polytypes within the group, or disordered sequences with lateral layer shifts of +b/3, −b/3, or no shift, where b is the b-axis vector for the orthohexagonal cell (Bailey, 1969, 1988).
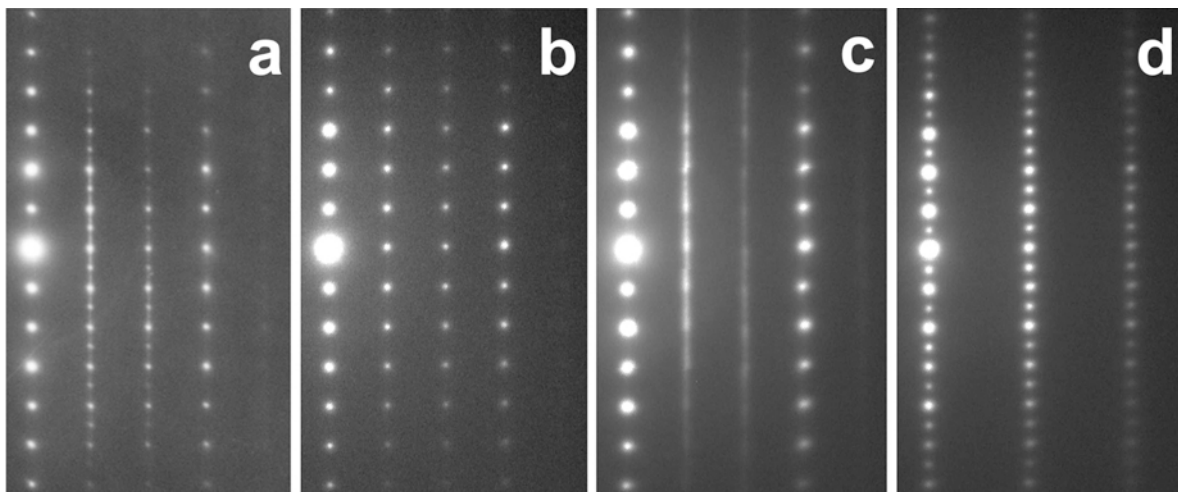
Figure 2. Selected-area electron diffraction (SAED) patterns from guidottiite with the incident beam along the (a−c) <100> and (d) <1$\bar{1}$0> directions. The diameter of the selected area was ~100 nm. The patterns in c and d were taken from the same area.

The HRTEM images (Figure 3) corresponding to these diffraction features are shown. Kogure *et al.* (2001) presented the interpretation of the contrast of similar images. More than forty layers (Figure 3a) show a stacking sequence with two-layer periodicity, comprising lateral staggers of alternating + $b/6$ and −$b/6$ from the preceding layer ("+" indicates the stagger to the right from the lower layer and − indicates that to the left). These "+$b/6$" and "−$b/6$" staggers correspond to the layer displacement of −$b/3$ and +$b/3$, respectively (Kogure *et al.*, 2001). In contrast, most layers (Figure 3b) show no stagger between adjacent layers, which results in one-layer periodicity. A disordered stacking sequence (Figure 3c) is clearly observed, in which lateral stagger of a layer from the preceding layer is disordered among +$b/6$ (expressed as +), −$b/6$ (−), or no shift (0). Finally, HRTEM images along the <1$\bar{1}$0> directions (Figure 3d) show ordered two-layer periodicity by contrast where the slant direction of the octahedra in each 1:1 layer is alternating along the stacking, confirming that the crystal structure belongs to group D (Bailey, 1988; Kogure *et al.*, 2001).

The EDS analysis was performed to determine if a different composition occurs for different polytypic features (Kogure *et al.*, 2002). The spectra from $2H_1$, $2H_2$, and disordered domains showed no significant difference with respect to the ratio of Mg, Si, Mn, and Fe, considering the accuracy in TEM-EDS analysis of ion-milled specimens. These spectra are more consistent with the Cameca-A probe results.

X-RAY CRYSTALLOGRAPHY

Powder pattern

A Gandolfi powder pattern (Table 1; data derived from JADE 8.5; MDI, 2006) was obtained using a

Bruker AXS D8 SMART/APEX three-circle diffractometer using monochromatized MoKα radiation (0.7107 Å) with a collimator aperture size of 0.3 mm and CCD detector with 1024×1024 pixel resolution and a crystal-to-detector distance of 120 mm following the procedure of Guggenheim (2005). The crystal used for the powder pattern was determined by precession photo techniques to apparently contain only the $2H_2$ polytype (see comments below, these crystals probably contain $2H_1$ components). However, the 00l reflections form a non-rational series because $d_{002 (calc)} > d_{002 (obs)}$, whereas $d_{004 (calc)} < d_{004 (obs)}$, further suggesting an intergrowth. The data showed preferred orientation, even with three different orientations of a single crystal. All material examined showed the presence of impurity phases.

Symmetry determination

Most crystals exhibit diffuse streaking of the $k \neq 3n$ reflections (orthohexagonal indexing) in Buerger precession photographs indicating stacking disorders along with intergrowth domains, and/or twinning effects. Many crystals were examined, and the crystals that initially displayed minimal or no streaking were further analyzed. By the precession method, the bulk sample contained crystals of at least two polytypes ($2H_1$ and $2H_2$) dominated by $2H_1$. The crystal chosen for X-ray study showed no streaking of the $k \neq 3n$ reflections in Buerger precession photographs, though a very small amount of streaking was observed from data collected by the high sensitivity of the CCD detector. No general systematic absences occur on the hkl nets (orthohexagonal indexing) indicating a primitive lattice and the $l = 2n$ reflections were systematically present on the 00l, indicating a 6_3-screw axis. Comparison of the $h0l$ precession photographs with calculated and observed $h0l$ photographs (Bailey, 1988) clearly indicated a $2H_2$
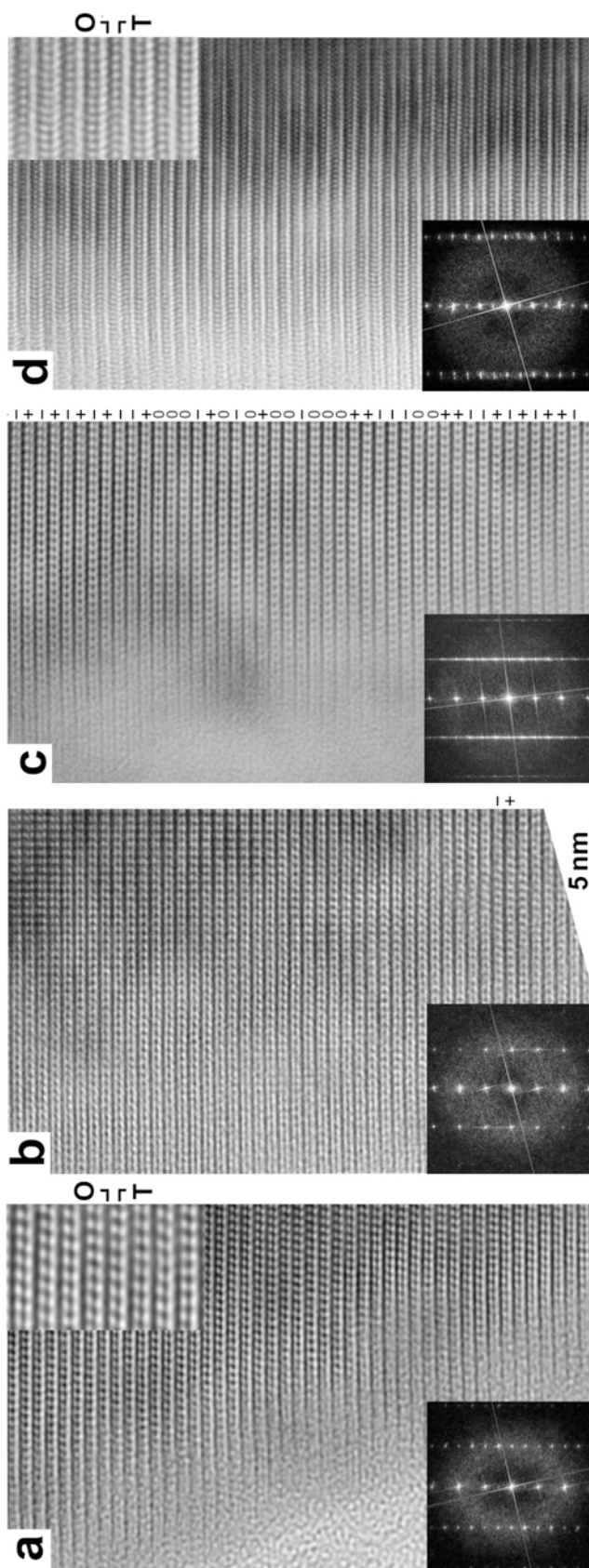
Figure 3. Filtered HRTEM images from guidottiite along the (a–c) <100> and (d) <1$\bar{1}$0> directions. The inset at the bottom-left of each figure is the Fourier transform of the image. The insets at the top-right in (a) and (d) are a portion of the images with greater magnification, and 'O' and 'T' indicate the positions of the octahedral and tetrahedral sheets, respectively, in a 1:1 layer. The characters 0, +, and − on the right of the images in (b) and (c) indicate lateral stagger of each layer from the preceding layer (Kogure *et al.*, 2001).

Table 1. X-ray powder diffraction data of guidottiite-$2H_2$.

d_{obs}	I_{obs}	d_{calc}	(hkl)	d_{obs}	I_{obs}	d_{calc}	(hkl)
7.21	100.0	7.15	(0 0 2)	1.374	6.9	1.378	(1 1 9)
4.82	8.0	4.80	(1 0 0)	1.358	3.7	1.357	(1 2 7)
4.58	5.6	4.55	(1 0 1)			1.329	(3 0 6)
3.99	5.6	3.99	(1 0 2)	1.326	5.4	1.327	(1 3 1)
3.543	50.4	3.574	(0 0 4)			1.325	(2 0 9)
3.328	4.4	3.383	(1 0 3)	1.243	2.8	1.248	(2 2 5)
2.848	2.3	2.868	(1 0 4)	1.194	1.3	1.193	(3 0 8)
2.706	13.8	2.723	(1 1 1)	1.172	1.8	1.177	(1,1,11)
2.568	38.8	2.586	(1 1 2)	1.144	2.9	1.143	(2,0,11)
2.381	25.1	2.397	(1 1 3)	1.093	3.8	1.096	(2 2 8)
		2.383	(0 0 6)			1.095	(1,1,12)
2.179	8.8	2.191	(1 1 4)	1.042	1.5	1.045	(2 2 9)
1.982	25.9	1.991	(1 1 5)	1.021	1.8	1.021	(0,0,14)
1.801	7.9	1.807	(1 1 6)			1.021	(3 1 9)
		1.801	(1 2 1)	0.982	2.0	0.984	(4 1 5)
1.640	12.0	1.645	(1 1 7)	0.931	1.9	0.933	(1 4 7)
1.595	10.2	1.601	(3 0 0)			0.930	(3,1,11)
1.558	6.1	1.556	(2 0 7)	0.902	2.0	0.904	(1 4 8)
1.498	10.3	1.502	(1 1 8)			0.904	(2,2,12)
1.456	7.7	1.461	(3 0 4)	0.873	1.0	0.873	(2,3,10)
1.423	1.8	1.430	(0,0,10)	0.860	1.7	0.861	(3,0,14)

Note: *d* values (Å) and Miller indices calculated using: $a = 5.5472(3)$, $c = 14.296(2)$ Å, and $P6_3$ symmetry. Collected using Gandolfi powder-pattern simulations (Guggenheim, 2005) and MoKα radiation. d_{obs},I_{obs} of 18.40,5.1; 10.95,2.9; 8.31,3.9; 3.82,5.1; and 1.951,5.4 are present in the pattern (not shown above) and are attributed to impurities.

polytype. The diffraction quality (*i.e.* lack of streaking, sharpness of spots) of $2H_2$ polytype crystals was superior to the $2H_1$ polytype crystals and, for this reason, the $2H_2$ polytype was used for data collection.

Data collection

The crystal used for refinement underwent X-ray diffraction analysis at the X-ray laboratory at the University of Notre Dame, South Bend, Indiana, USA, and the data were recollected at the Bruker-AXS X-ray Laboratory in Madison, Wisconsin, USA. Both datasets produced the same results, and therefore only the Bruker-AXS data set is described here. The crystal was lost in transit before the dimensional size of the crystal was measured.

The crystal was mounted on a Bruker three-circle diffractometer with a crystal-to-detector distance of 6 cm. The data were collected using a graphite-monochromatic MoKα X-ray radiation with framewidths of 1.5° in ω (120 s per frame) and *SMART* software. Data were collected for 3° < 2θ < 55° over ~15 h. The three-dimensional data were reduced and filtered for statistical outliers using the Bruker program *SAINT*. An absorption correction was applied using the multirun technique and the data were corrected for Lorentz polarization and background effects. A total of 3261 reflections were collected.

Refinement

The University of Illinois, Chicago (UIC) crystallography lab was undergoing both instrumentation (from Picker to Bruker equipment) and software [from *SDPWIN* (Frenz, 1997) to *SHELXTL* (Sheldrick, 1997)] changes during the period when guidottiite was being studied. Thus, the refinement was performed using *SDPWIN* and, to a lesser extent, *SHELXTL*.

The refinement of guidottiite was first attempted in space group $C1$ to account for possible subgroup (distorted hexagonal) symmetry, because Geiger *et al.* (1983) suggested that the symmetry of cronstedtite was not hexagonal. However, the refinement process was unstable, and thus the symmetry of the crystal was too high to be refined in this space group. Consequently, cell parameters referred to the C-centered cell were collected on a Picker FACS1 diffractometer using Mo radiation and 21 reflections resulted in values of $a = 5.543(4)$, $b = 9.595(8)$, $c = 14.281(9)$ Å, $\alpha = 89.93(3)$, $\beta = 90.04(3)$, and $\gamma = 89.91(7)^o$, which are comparable to the cell determined by Geiger *et al.* (1983) for cronstedtite. The standard deviation of each angle for guidottiite is <3σ for both the cell determinations presented here and by Geiger *et al.* (1983), suggesting that the ideal hexagonal cell adequately describes the hexagonal symmetry, metric size, and shape of the unit cell for both minerals.

The 3261 reflections were symmetrically averaged to 656 unique reflections ($R_{int} = 0.025$) with 631 observed reflections (I > 3σI) in space group $P6_3$ and cell dimensions of $a = 5.5472(3)$ and $c = 14.296(2)$ Å [$V = 380.98(6)$ Å^3]. Idealized atomic coordinates for a $2H_2$ polytype (Bailey, 1969) were initially used and scattering factor curves in *SDPWIN* were taken from the

International Tables assuming half-ionized atoms. All reflections were assigned a unit weight, and a single scale factor was used. In the early stages of the refinement, isotropic displacement factors of B = 0.6, 0.8, and 1.5 Å^2 were assigned to the tetrahedral (T), octahedral (M), and anion (O, OH) sites, respectively, in the asymmetric unit, and the origin was fixed at the basal oxygen atom site (O1). The tetrahedral (Si, Fe) and octahedral cations (Mn, Mg, and Fe) were assumed disordered and the refinement was performed using F^2.

Initial least-squares cycles varying the scale factor, atomic coordinates, site multipliers, and isotropic displacement factors were performed resulting in R_1 = 0.066 (R_1 = Σ(|F$_o$| − |F$_c$|) / Σ|F$_o$|) and wR = 0.104 (wR = [Σw(|F$_o$| − |F$_c$|)^2 / Σw|F$_o$|^2]$^{1/2}$, w = 1.0). At this stage, the isotropic displacement parameter (B) of the basal oxygen atom was large at 4.9 Å^2, indicating probable positional disorder.

The Fourier electron density map indicated an electron density suggesting ordering in the tetrahedral sites (probe analysis = 16.0 electrons, Fourier: T1 = 19.4 electrons, T2 = 13.7 electrons). Complete ordering (based on the Cameca-Y microprobe chemistry) of Fe^{3+} was the first model used (occupancy ratio Si^{4+}:Fe^{3+} = 0.366:0.634 in T1 and 1.0:0.0 in T2); however, electron density maps indicated a variance from the electron microprobe data and partial ordering. The final occupancy ratios, which varied moderately from the microprobe analysis for the tetrahedral sites as derived from the refinement, are Si^{4+}:Fe^{3+} = 0.406:0.594 in T1 and 0.868:0.132 in T2, which corresponds to an approximate bulk tetrahedral composition of Si$_{1.27}$Fe$^{3+}_{0.73}$. This suggests that ordering of Fe^{3+} is not complete but that Fe^{3+} is preferentially partitioned into T1. The Fourier electron density map showed an electron density inconsistency with the probe analysis (probe = 21.8 electrons, isotropic refined value = 27 electrons) in the octahedral (M) site. The composition of the octahedral site could not be refined to produce meaningful results; therefore, the composition of the octahedral site was constrained to that derived from the (Cameca-Y) electron microprobe.

After varying anisotropic displacement parameters along with the scale factor for one cycle, all parameters were varied together (R_1 = 0.052 and wR = 0.075 on F^2). The refinement did not converge smoothly and parameter shifts were relatively large. The final R factors, when using F instead of F^2, are R = 0.045 and wR = 0.041. This refinement behaved similarly to that using F^2. An examination to determine the correct absolute enantiomorphic configuration was performed and resulted in elevated R factors (R_1 = 0.063 and wR = 0.087); therefore, the present configuration was maintained.

At this point, the two highest difference map peaks (x = 0.3320, y = 0.6660, z = 0.5410, at 4.5 electrons/Å^3 and x = 0.2070, y = 0.8750, z = 0.50, at 3.5 electrons/Å^3) occurred at approximately the same z coordinate of the

tetrahedral cation plane and basal oxygen atom plane in the upper layer of the 2H_2 polytype, respectively (referred to as 'apparent' cation/anion). The apparent tetrahedral cation projected onto the OH1 site and was located 1.723 Å away from the apparent basal oxygen atom, which did not project onto any 2H_2 atom sites. Because the apparent tetrahedral cation projected directly onto the OH1 site, this was interpreted as domains that are shifted by a fixed amount within the crystal. To acquire a sense of the shift of the domains relative to each other, comparisons were made between the apparent atom sites (in the upper layer) and the bottom layer of the 2H_2 polytype. The apparent tetrahedral cation projected directly over the T2 site and the apparent basal oxygen atom projected adjacent to one of the basal oxygen atoms coordinated to the T2 site. From this, evidence suggests that: (1) if the difference map peaks correspond to tetrahedral and basal oxygen atoms, then one domain within the crystal is 2H_2, where the top layer is shifted by b/3 in relation to the bottom layer, and the other domain has zero shift between the layers; and (2) because the apparent basal oxygen atom does not project directly over the basal oxygen atom of the bottom layer, this may account for the large value of the O1 displacement parameter. Clearly, the superfluous peaks belong to domains containing 2H_1. Thus, the upper layer of the 2H_1 differs in position from the upper layer of the 2H_2 polytype, but the bottom layers of the 2H_1 and 2H_2 are nearly identical and superpose.

Refinements (*SPDWIN* and *SHELXTL* gave the same results to significant places) were performed where the Fourier difference map peaks attributed to the 2H_1 polytype tetrahedral cation and basal oxygen atom were included. In *SDPWIN*, the R-factors dropped to R = 0.040 and wR = 0.058. However, the resulting 2H_1 T−O bond length error (1.660±0.042 Å) was considered too large to accurately determine the composition of the 2H_1 tetrahedral site.

To compensate for the close proximity of the 2H_1 and 2H_2 bottom-layer basal oxygen atoms, another refinement was initiated. This refinement followed the same procedures as described above, with the exception of the treatment of the O1 displacement parameter, which was refined isotropically (B refined value was 4.9 Å^2), but held constant at B = 1.5 Å^2 (U_{eq} = 0.0190). The final refinement was stable resulting in R_1 = 0.072 and wR = 0.108. Atomic coordinates (Table 2, data derived from *SDPWIN*) and calculated bond lengths and angles (Table 3, data derived from *SDPWIN*) are presented. As expected, the R-factors increased compared to the refinement where B of O1 was refined (R_1 = 0.052 and wR = 0.075) because of the limitation on the O1 displacement factor. The refinement resulted in occupancy ratios for the tetrahedral sites of: Si^{4+}:Fe^{3+} = 0.207:0.793 in T1 and 0.697:0.303 in T2 (approximate bulk composition Si$_{0.90}$Fe$^{3+}_{1.10}$).

Table 2. Atomic coordinates (labels follow Bailey, 1969, Table 1) and displacement factors for guidottiite-$2H_2$ in space group $P6_3$.

Atom	x	y	z	U_{eq}*	U_{11}	U_{22}	U_{33}	U_{12}	U_{13}	U_{23}
M1	0.6670(2)	−0.0008(2)	0.2375(1)	0.0139	0.0138(3)	0.0138(3)	0.0141(4)	0.0070(3)	0.0001(4)	0.0003(4)
T1	0	0	0.0382(3)	0.0165	$2U_{12}$	$2U_{12}$	0.0097(9)	0.0043(1)	0	0
T2	1/3	2/3	0.0366(4)	0.0177	$2U_{12}$	$2U_{12}$	0.011(1)	0.0044(2)	0	0
O1	0.191(2)	0.332(2)	0	0.0190	**					
O4	0	0	0.1570(7)	0.0152	$2U_{12}$	$2U_{12}$	0.001(4)	0.0048(8)	0	0
O5	1/3	2/3	0.1577(7)	0.0139	$2U_{12}$	$2U_{12}$	0.007(4)	0.0037(7)	0	0
OH1	2/3	1/3	0.1592(7)	0.0114	$2U_{12}$	$2U_{12}$	0.002(4)	0.0034(7)	0	0
OH2	0.335(1)	0.001(1)	0.3081(4)	0.0089	0.010(2)	0.013(2)	0.002(2)	0.005(2)	0.002(2)	0.001(2)

* Isotropic equivalent displacement factor
** Value not refined
Note: Displacement parameters of the form:
$\exp[-2\pi^2(U_{11}h^2\mathbf{a}^{*2} + U_{22}k^2\mathbf{b}^{*2} + U_{33}l^2\mathbf{c}^{*2} + 2U_{12}hk\mathbf{a}^*\mathbf{b}^* + 2U_{13}hl\mathbf{a}^*\mathbf{c}^* + 2U_{23}kl\mathbf{b}^*\mathbf{c}^*)]$

Refinement in space group $P6_3cm$

Ďurovič *et al.* (2004) noted that cronstedtite-$1T$ commonly contains parallel intergrowths and suggested ways to manipulate scale factors to account for the intergrowth. The procedure is not suitable for an intergrowth of $2H_2$ and $2H_1$ polytypes because these polytypes have different symmetries and should not be refined together with multiple scale factors, and because streaking of k ≠ 3n reflections is minimal (*i.e.* no

physical reason for the procedure). However, because of the similarity of structure between the $2H_2$ and $2H_1$ polytypes (assuming identical composition and cell dimensions as indicated by TEM), the refinement was attempted in space group $P6_3cm$ (*i.e.* assuming a $2H_1$ polytype only, omitting *c* glide absences to conform to the space group). Idealized atomic coordinates for a $2H_1$ polytype were initially used (Bailey, 1969) and the cell dimensions of the $2H_2$ ($P6_3$) refinement were used. The same initial steps implemented for the $P6_3$ refinement

Table 3. Calculated bond lengths (Å), angles (°), and structural parameters.

Octahedral							
M1−OH2	2.105(4)		Unshared			Shared	
−OH2	2.107(5)		OH2−OH2	3.190(7)		OH1−OH2 (×2)	2.815(9)
−OH2	2.108(5)		O4−O5	3.203(0)		O5−OH2 (×2)	2.837(9)
−OH1	2.166(5)		O4−OH1	3.203(0)		O4−OH2 (×2)	<u>2.848(9)</u>
−O5	2.172(5)		O5−OH1	3.203(0)		Average:	2.833
−O4	2.175(5)		OH2−OH2	3.204(7)			
Average:	2.139		OH2−OH2	3.214(5)			
			Average:	3.203			

	About M1		About M1				
	O4−O5	94.9(2)	O5−OH2	83.1(2)		Interlayer contact	
	O4−OH1	95.1(2)	OH1−OH2	82.4(2)		OH2−O1	2.854(6)
	O4−OH2	83.3(2)	OH1−OH2	82.5(2)			
	O4−OH2	83.4(2)	OH1−OH2	177.5(3)		Tetrahedral rotation angle (α)	
	O4−OH2	177.0(3)	OH2−OH2	177.0(3)		9.9(3)	
	O5−OH1	95.2(2)	OH2−OH2	99.0(2)			
	O5−OH2	83.1(2)	OH2−OH2	98.5(2)			

Tetrahedral						
T1−O1 (x3)	1.692(9)				About T	
−O4	1.70(1)		O1−O1 (×3)	2.773	110.1(4)	
Average:	1.694		O1−O4 (×3)	2.757	108.9(2)	
T2−O1 (×3)	1.696(9)				About T	
−O5	1.73(1)		O1−O1 (×3)	2.795	110.9(4)	
Average:	1.705		O1−O5 (×3)	2.773	108.0(2)	

were performed and the refinement resulted in $R = 0.114$ and $wR = 0.206$ ($R = 0.066$ and $wR = 0.104$ for the $2H_2$ at this stage of refinement), further indicating that space group $P6_3$ is correct. The largest peak in the Fourier difference map ($x = 0.0$, $y = 0.0$, $z = 0.5332$) had a z-coordinate approximately the same as the tetrahedral cation plane. After relating the origin of the $2H_2$ and $2H_1$ polytypes, this peak undoubtedly represents the non-overlapping T2 site of the $2H_2$ polytype. The results of this refinement are analogous to the results of the $P6_3$ refinement, which is consistent with the crystal containing an interstratified mixture of $2H_1$ and $2H_2$ polytypes and the composition and cell dimensions of the two polytypes being similar.

RESULTS AND DISCUSSION

Twinning considerations

Before the O1 displacement parameter was held constant, several problematic issues occurred which involved the relationship between the chemical composition of the sample and the X-ray refinement. These issues were: (1) the observed mean tetrahedral bond lengths varied significantly from values calculated from probe data and from the ideal $^{IV}Fe^{3+}-O$ and $^{IV}Si^{4+}-O$ bond lengths of 1.85 Å and 1.62 Å, respectively; (2) T$-O_{apical}$ bond distances were considerably elongated, and (3) the values of the displacement parameters for O1 refined to unreasonably large values (B = 4.9 Å^2). Similar issues (Table 4) were observed in the refinements of the Fe-rich analogue, cronstedtite (Geiger *et al.*, 1983; Smrčok *et al.*, 1994; Hybler *et al.*, 2000; Hybler *et al.*, 2002). In addition, the Flack index was ~0.14, suggesting a possible twin or intergrowth with superposed reflections.

The possibility of twinned crystals was studied using a specialized program for twinned crystals (*TWINABS*, Bruker, 2001) by Dr Michael Ruff, Bruker-AXS, Madison, Wisconsin, USA. The refinement indicated the possible presence of merohedral twinning with a twin law of (010/100/00$\bar{1}$). However, this twin law requires domain boundaries where 1:1 layers are oriented with octahedral sheets adjacent to other octahedral sheets, or tetrahedral sheets adjacent to other tetrahedral sheets, or insertion of 2:1 layers. The TEM analyses of crystals from the bulk sample did not find such structures, and thus the prospect of such twinning is unlikely.

The cronstedtite-$2H_2$ polytype refinement by Hybler *et al.* (2002) considered other twin models, namely (010/100/001) and ($\bar{1}$00/0$\bar{1}$0/00$\bar{1}$). The twin law of (010/100/001) appears to be the most promising for the present X-ray study based on the TEM analyses of guidottiite because this twin law does not involve adjacent octahedral-to-octahedral sheets or tetrahedral-to-tetrahedral sheets. However, all three twin models produced nearly identical R values for guidottiite. Therefore,

Table 4. Comparison of guidottiite T$-O_{apical}$ and mean T$-O_{basal}$ bond distances to other similar studies.

		Geiger *et al.* (1983)*	Smrčok *et al.* (1994)**	Hybler *et al.* (2000)*** Herja	Hybler *et al.* (2000)*** Lostwithiel	Hybler *et al.* (2002)[†] Wheal Maudlin	Hybler *et al.* (2002)[†] Pribram	Guidottiite[‡]	Guidottiite[§]
T1	O_{apical}	1.676(8)	1.757(5)	1.736(3)	1.756(3)	1.725(6)	1.726(4)	1.7047	1.70(1)
	O_{basal}	1.678	1.705	1.715(1)	1.704(1)	1.682(4)	1.680(4)	1.6746	1.692(9)
	difference	−0.002	0.052	0.021	0.052	0.043	0.046	0.0301	0.008
T2	O_{apical}	1.754(9)	1.757(5)			1.795(6)	1.765(4)	1.7614	1.73(1)
	O_{basal}	1.645	1.710			1.722(6)	1.728(3)	1.6918	1.696(1)
	difference	0.109	0.047			0.073	0.037	0.0696	0.034
T11	O_{apical}	1.694(8)							
	O_{basal}	1.666							
	difference	0.028							
T22	O_{apical}	1.776(8)							
	O_{basal}	1.658							
	difference	0.118							

* cronstedtite-$2H_2$ in C1; ** cronstedtite-$3T$ in $P3_1$; *** cronstedtite-$1T$ in $P31m$
[†] cronstedtite-$2H_2$ in $P6_3$; [‡] Refinement results before O1 displacement held constant
[§] Final refinement results (O1 displacement held constant)

without additional guidottiite TEM data, no one model can be favored over the other. Although these refinements were stable, produced smaller values (from $U_{eq} = 0.070$ to 0.038 Å^2) of the anisotropic displacement parameters for the basal oxygen atom (O1), and decreased the T$-$O$_{apical}$ bond lengths, further study of the twinning models was abandoned because these models did not resolve the issue associated with the tetrahedral compositions. The results obtained here (see below) suggest that an intergrowth model better explains both the apparent compositional effects and the large refined displacement factor of the O1 basal oxygen atom.

$2H_1$ polytype intergrowth

Atomic coordinates for the $2H_1$ polytype (Bailey, 1969) and the cell dimensions of guidottiite-$2H_2$ were used to plot the upper layer of the $2H_1$ polytype (Figure 4). After relating the origin of the $2H_1$ and $2H_2$ polytypes, the $2H_1$ polytype was compared to a model containing the two largest peaks obtained from the residual difference map of the $2H_2$ refinement. The apparent tetrahedral atom of the $2H_1$ polytype projected directly onto a T site and the apparent basal oxygen atom projected next to a basal oxygen atom of the $2H_1$ model, indicating that the difference peaks were a consequence of the presence of a $2H_1$ domain (Figure 4), which is also in accord with the TEM data. Half of the tetrahedral sites in the $2H_1$ top layer superpose over half of the tetrahedral sites in the $2H_2$ top layer (T1 sites only). This relationship causes the electron densities of the T1 site to have an excess of electrons relative to the T2 site.

The $2H_1$ ($P6_3cm$) refinement, where only one unique T site exists, has a T$-$T cation distance of 3.20 Å. Similarly, the $2H_2$ ($P6_3$) polytype, where two unique T sites exists, has a T$-$T distance that is equivalent, also at 3.20 Å. Thus, from both X-ray and TEM data, the tetrahedral compositions of the two structures are nearly identical. Nonetheless, the observed electron densities at the T sites of the $2H_2$ polytype are not consistent with this conclusion, and this suggests additional evidence of an intergrowth. Furthermore, in all the cronstedtite refinements to date, the bulk observed T$-$O bond lengths are in good to excellent agreement with the predicted values from the bulk tetrahedral composition derived from microprobe analyses (Table 4).

In summary, the crystal under X-ray study contains domains of primarily two structure types and the space group symmetry of each is different. The TEM analysis also suggests the presence of these two polytypes. (1) The sites of the $2H_1$ polytype differ in position relative to the sites of the $2H_2$ polytype and result in large R factors because site occupancies of both cannot be considered simultaneously in a single refinement using the present software. Between the two polytypes complete overlap of the octahedral sites, some overlap of the tetrahedral sites, and some overlap of oxygen atoms

occurs. (2) Sites related to the two polytypes with very similar or identical positions in the average unit cell result in an apparent excess of electrons. This occurs for the T1 sites ($2H_2$ polytype), but not the upper-layer apical oxygen atoms (O4).

Bond lengths

In contrast to the previous studies of cronstedtite where determining cation compositions from the refinement relied on electron-density values, the observed electron-density values are misleading because of previously unrecognized polytype intergrowths. The electron counts of the T sites of the $2H_2$ polytype are
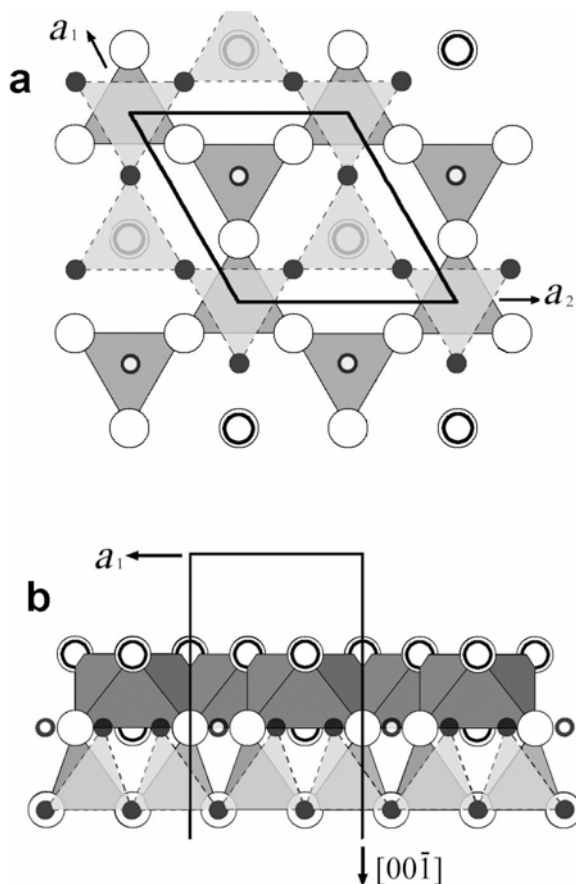

Figure 4. The upper layer of the $2H_1$ domain (origin referred to $2H_2$) projected onto the upper layer of the guidottiite-$2H_2$ unit cell (a) along [00$\bar{1}$] and (b) [010]. Large open circles represent oxygen atoms and large double circles represent hydroxyls of the $2H_2$ polytype; small filled circles represent oxygen atoms and small open circles represent hydroxyls of the $2H_1$ polytype. The $2H_1$ polytype is shown as dashed, outlined, translucent tetrahedra. (1) The $2H_1$ basal oxygen atoms do not overlap any $2H_2$ atoms, (2) half of the $2H_1$ T1 sites overlap T sites of the $2H_2$ (one quarter from each of the unit cell corners), (3) the T1 and OH1 sites of the $2H_1$ in the center of the unit cell projects onto the OH1 and T2 sites of the $2H_2$, respectively, and (4) the upper-layer octahedra of both polytypes overlap.

T1 = 21.9, T2 = 15.8 electrons, and these electron counts are inconsistent with the microprobe analysis and bond-length values. Using bond lengths, the composition of the tetrahedral sites of the $2H_1$ polytype is consistent with the results of the microprobe analysis. Because displacement parameters and multipliers absorb errors in the data set (Massa, 2004), particularly for a data set consisting of two domains, bond lengths are a better indicator than refined atom multiplier values to determine site occupancy.

Based on the observed mean T−O bond lengths (T1 = 1.694, T2 = 1.705 Å), the tetrahedral cation compositions of T1 and T2 are nearly equal (considering the standard deviations and quality of the refinement). The resulting composition is $(Si^{4+}:Fe^{3+})$ = 0.678:0.322 in T1 and 0.631:0.369 in T2. The approximate bulk composition, based on the bond lengths, of $Si_{1.31}Fe^{3+}_{0.69}$ is in good agreement with the microprobe analysis of $Si_{1.36}Fe^{3+}_{0.64}$.

The observed M−O,OH mean bond length (2.139 Å) is in excellent agreement with the microprobe chemistry (2.135 Å), assuming ideal bond lengths (Shannon, 1976). However, similar to the problems associated with the electron densities in the tetrahedral sites, the electron densities of the octahedral site (28.2 electrons) do not agree with the observed mean bond lengths and microprobe chemistry (22 electrons). This problem is attributed to the differently diffracting domains of $2H_1$ and $2H_2$ polytypes that comprise the crystal under study.

CONCLUSIONS

The results of the guidottiite refinement appear very similar to the results of the cronstedtite-$2H_2$ refinements (Geiger *et al.*, 1983; Hybler *et al.*, 2002). Similar to guidottiite, many single-crystal refinements of cronstedtite minerals exhibit ±*b*/3 out-of-step domains, though the domains were previously thought to be related to twinning and to be of the same symmetry as the main structure. Cronstedtite-$2H_2$ single-crystal refinements also exhibit large O1 displacement parameters, large elongated $T2-O_{apical}$ bond lengths and moderately elongated $T1-O_{apical}$ bond lengths, and observed mean tetrahedral bond lengths that do not agree with the observed electron densities associated with the sites; all similar to the guidottiite refinement. The two cronstedtite-$2H_2$ single-crystal refinements by Hybler *et al.* (2002) included twinning matrices in the refinement procedures, which significantly reduced the O1 displacement parameters and reduced the $T-O_{apical}$ bond lengths to somewhat more reasonable values. However, for each refinement, the displacement parameter values were still considerably larger compared to the other oxygen atoms and the $T-O_{apical}$ bond lengths were still moderately elongated.

Problems arise with the entire data set where differently diffracting domains of $2H_1$ and $2H_2$ polytypes comprise the crystal under study. A portion of the

intensity for each, or nearly each, *hkl* value results from the $2H_1$ polytype. Specifically, the intensities are significantly influenced along the reciprocal rows with $h-k \neq 3n$ (Hybler *et al.*, 2002). Furthermore, the differences between symmetrically averaging the data in $P6_3$ *vs.* $P6_3cm$ symmetry produce additional problems in relation to the intensities of the *hkl* values. A portion of each F_o value in the $P6_3$ refinement is affected by contributions from the $2H_1$ polytype. Thus, the intensity components contributed by the $2H_1$ polytype were averaged symmetrically in an incorrect ($P6_3$) space group. The displacement parameters, and to a lesser extent the multiplicities, appear to absorb much of the error resulting from these effects.

Given the universally comparable problems associated with single-crystal cronstedtite-$2H_2$ refinements, the evidence suggests that cronstedtite-$2H_2$ polytype could be frequently, if not universally, associated with cronstedtite-$2H_1$ polytype. This association has been found in the guidottiite crystal used in this study along with other crystals in the sample revealed by the TEM analyses. The association has also been described in the cronstedtite crystals from Kutná Hora (Kogure *et al.*, 2001). The cronstedtite-$2H_2$ single-crystal refinement by Geiger *et al.* (1983) referred to domains consisting of an ordered $2H_1$ polytype; those authors, however, did not investigate the consequences of this further. The two cronstedtite-$2H_2$ single-crystal refinements by Hybler *et al.* (2002) did not identify domains consisting of $2H_1$ polytypes. However, they did state the possibility of this occurrence, but were unable to investigate adequately because of the complexity of the problem.

REFERENCES

Bailey, S.W. (1969) Polytypism of trioctahedral 1:1 layer silicates. *Clays and Clay Minerals*, **17**, 355−371.
Bailey, S.W. (1988) X-ray diffraction identification of the polytypes of mica, serpentine, and chlorite. *Clays and Clay Minerals*, **36**, 193−213.
Bloss, F.D. (1971) *Crystallography and Crystal Chemistry, An Introduction*. Holt, Rinehart and Winston, Inc., New York.

Broz, M.E., Cook, R.F., and Whitney, D.L. (2006) Microhardness, toughness, and modulus of Mohs scale minerals. *American Mineralogist*, **91**, 135−142.

Bruker AXS, Inc. (2001) *TWINABS*. Madison, Wisconsin, USA.

Dornberger-Schiff, K. and Ďurovič, S. (1975) OD-interpretation of kaolinite-type structures − II. The regular polytypes (MDO-polytypes) and their derivation. *Clays and Clay Minerals*, **23**, 231−246.

Ďurovič, S., Hybler, J., and Kogure, T. (2004) Parallel intergrowths in cronstedtite-1*T*: Implications for structure refinement. *Clays and Clay Minerals*, **52**, 613−621.

Frenz, B.A. (1997) *SDP for Windows*. College Station, Texas, USA.

Geiger, C.A., Henry, D.L., Bailey, S.W., and Maj, J.J. (1983) Crystal structure of cronstedtite-2H_2. *Clays and Clay Minerals*, **31**, 97−108.

Guggenheim, S. (2005) Simulations of Debye-Scherrer and Gandolfi patterns using a Bruker SMART/APEX Diffractometer system. *Bruker-AXS Application Note 373*, 8. Madison, Wisconsin, USA (see also American Crystallographic Annual Meeting, Chicago, Illinois, July, 2004, abstract, 182).

Guggenheim, S. and Koster van Groos, A.F. (1992) High-pressure differential thermal analysis (HP-DTA): I. Dehydration reactions at elevated pressures in phyllosilicates. *Journal of Thermal Analysis*, **38**, 1701−1728.

Hybler, J., Petříček, V., Ďurovič, S., and Smrčok, L. (2000) Refinement of the crystal structure of cronstedtite-1*T*. *Clays and Clay Minerals*, **48**, 331−338.

Hybler, J., Petříček, V., Fábry, J., and Ďurovič, S. (2002) Refinement of the crystal structure of cronstedtite-2H_2. *Clays and Clay Minerals*, **50**, 601−613.

Kilaas, R. (1998) Optimal and near-optimal filters in high-resolution electron microscopy. *Journal of Microscopy*, **190**, 45−51.

Kogure, T. (2002) Investigation of micas using advanced TEM. Pp. 281−310 in: *Micas: Crystal Chemistry & Metamorphic Petrology* (A. Mottana, F.P. Sassi, J.B. Thompson, Jr. and S. Guggenheim, editors). Reviews in Mineralogy and Geochemistry Vol. **46**, Mineralogical Society of America, Washington, D.C.

Kogure, T., Hybler, J., and Ďurovič, S. (2001) A HRTEM study of cronstedtite: Determination of polytypes and layer polarity in trioctahedral 1:1 phyllosilicates. *Clays and Clay Minerals*, **49**, 310−317.

Kogure, T., Hybler, J., and Yoshida, H. (2002) Coexistence of two polytypic groups in cronstedtite from Lostwithiel, England. *Clays and Clay Minerals*, **50**, 504−513.

Kogure, T., Eilers, P.H.C., and Ishizuka, K. (2008) Application of optimum HRTEM noise filters in mineralogy and related sciences. *Microscopy and Analysis*, **22**, S11−S14.

Koster van Groos, A.F. (1979) Differential thermal analysis of the system NaF-Na$_2$CO$_3$ to 10 kbar. *Journal of Physical Chemistry*, **83**, 2976−2978.

Marks, L.D. (1996) Wiener-filter enhancement of noisy HREM images. *Ultramicroscopy*, **62**, 43−52.

Massa, W. (2004) *Crystal Structure Determination*. Springer-Verlag Press, Berlin.

MDI, Materials Data, Inc. (2006) *JADE* 8.5. Livermore, California, USA.

Schissel, D. and Aro, P. (1992) The Major Early Proterozoic Sedimentary Iron and Manganese Deposits and their Tectonic Setting. *Economic Geology and the Bulletin of the Society of Economic Geologists*, **87**, 1367−1374.

Shannon, R.D. (1976) Revised effective ionic-radii and systematic studies of interatomic distances in halides and chalcogenides. *Acta Crystallographica Section A*, **32**, 751−767.

Sheldrick, G.M. (1997) *SHELXTL97 version 5.1: Program for the Solution and Refinement of Crystal Structures*. University of Göttingen, Germany.

Smrčok, L., Ďurovič, S., Petříček, V., and Weiss, Z. (1994) Refinement of the crystal structure of cronstedtite-3*T*. *Clays and Clay Minerals*, **42**, 544−551.

Zvyagin, B.B. (1962) Polymorphism of double-layer minerals of the kaolinite type. *Soviet Physics, Crystallography*, **7**, 38−51.